

# Discovery of monochromatic oscillations in optical spectrum of the intermediate polar RE 0751+14<sup>\*</sup>

N.N. Somov<sup>1</sup>, T.A. Somova<sup>1</sup>, and I.D. Najdenov<sup>1</sup>

Special Astrophysical Observatory of the Russian AS, Nizhniy Arkhyz 357147, Russia (som@sao.ru)

Received 9 September 1996 / Accepted 26 November 1997

**Abstract.** We report the results of optical dynamic spectroscopy and spectropolarimetry of the intermediate polar RE 0751+14 which were obtained with the help of the multichannel photon-counting system (scanner) in a high time resolution mode (32 ms) at the 6 m telescope (BTA) from February 1993 to March 1996. The dependences of the power of oscillations on the wavelengths (3900–5200 Å, 1 Å/channel) and periods of pulsations in the region 300–2000 s with a mean resolution along the period 10 s have been investigated. The statistically significant (the probability of random signal is till  $10^{-13}$ ) perturbations of spectral composition of the photoelectron noise in the narrow wavelength passbands (1 Å) were discovered. Power spectra have revealed strong (amplitude up to 40%), circularly polarized (dominating in one polarization) monochromatic (FWHM in power spectra 2–3 Å) oscillations with periods of 13.3–15.2 min in the vicinity of the spin period of the white dwarf (13.9 min) mainly in the profiles of emission lines with the time of life 3000–5000 s. The wavelengths of the oscillations correspond to the solutions of the Schrödinger equation in strong resonance magnetic fields (quadratic Zeeman effect). The equation for calculations of resonance magnetic fields for  $\sigma$  transitions is the equality of the wavelength shifts due to the linear and quadratic terms of the Zeeman effect. As a result of the detection of the oscillations corresponding to  $\sigma$ – transitions, the resonance magnetic fields equal for strongest transitions of  $H\delta \approx 4$  MGs and for  $H\gamma \approx 9$  MGs were measured. The strong magnetic fields indicate that the sources of radiation causing the oscillations are in the accretion column of the white dwarf. On the basis of analysis of properties of the oscillations we conclude that the physical nature of the sources of the oscillations and its radiation cannot be explained in frame of a conventional physics.

**Key words:** white dwarfs – accretion – stars: individual: RE 0751+14 – stars: oscillations – polarization – stars: magnetic fields

---

*Send offprint requests to:* N.N. Somov

<sup>\*</sup> Based on observations from Special Astrophysical Observatory of Russian Academy of Sciences, Russia

## 1. Introduction

The class of cataclysmic variables (CVs) presents semidetached binary systems consisting of a white dwarf primary star and a Roche lobe-filling late-type dwarf secondary star. The subclass of CVs known as DQ Her stars or intermediate polars (IPs) includes the objects containing an accreting, magnetic, rapidly nonsynchronously rotating white dwarf. The magnetic field of the white dwarf in IPs is strong enough (0.1–4 MGs) to disrupt the inner part of the normal accretion disk and to cause matter channelling towards the surface of the white dwarf in the vicinity of the magnetic poles. In the standard model of DQ Her stars the white dwarf’s spin and magnetic axes are not aligned and the star is an “oblique magnetic rotator”. The period of rotation of the white dwarf is less or usually much less than the orbital period of the system. The principal criterion for membership in this class (IPs) of stars is the presence of a rapid, highly coherent periodicity in a light curve, usually at optical or X-ray wavelengths. Stability of period and phase on very long time scales is essential, in order to distinguish the signals from more common quasiperiodic oscillations and flickering in the light curves. A recent review of properties of DQ Her stars has been made by Patterson (1994).

RE 0751+14 is a new magnetic CV discovered in the extreme-ultraviolet (70–200 Å) all-sky survey by the UK Wide Field Camera on the ROSAT satellite (Mason et al. 1992). The object has been studied from X-ray to infrared bands and has been classified as an intermediate polar. Most part of these observations have detected a 13.9 min period of variation of the light curves (Helditch & Bell 1994; Hellier et al. 1994). Optical spectral observations have shown a variability of the V/R ratio of emission lines over the spin period (Rosen et al. 1993). Polarimetric observations (Piirola et al. 1993) have not revealed significant polarization effects in U, B and V bands, but the circular and linear polarization, modulated with a 13.9 min period in R and I bands, has been discovered and a strong magnetic field (8–18 MGs) was indicated. The periodicity (13.9 min) was attributed to the rotation period of the white dwarf in the system. An ephemeris for this pulsation, which is quasi-sinusoidal in the blue and double-peaked in the red, was presented by Hellier et al. (1994). An additional period of 14.5 min in the light curves

**Table 1.** Parameters of observations

Instrumentation	: 6 m telescope+analyzer of :circular polarization+ :spectrograph SP124 + photon- : counting system (BTA scanner)
Object	: RE 0751+14
Classification	: CV (Intermediate polar)
Coordinates RA (2000)	: 07 51 17.3
DEC(2000)	: +14 44 23
V magnitude	: 14.6 mag
Observations	: February, 1993 - March, 1996
Wavelength region	: 3900-5200 Å
Dispersion	: 1 Å/channel
Time resolution	: 32 ms
Time of the exposures	: 1200-5400 s

implies an orbital period of about 5-6 hours. The spin-modulated polarization and the strong magnetic field make RE 0751+14 a peculiar intermediate polar and an interesting object for further studies.

The purpose of our paper is to investigate spectral and spectropolarimetric characteristics of the optical oscillations of RE 0751+14 in the vicinity of the spin period (13.3-15.2 min).

## 2. Observations

RE 0751+14 was observed at the Special Astrophysical Observatory (Nizhnij Arkhyz, Russia) from February 1993 to March 1996 (see the journal of observations in Table 2). Spectroscopic observations were performed in 1993, 1994 using the SP-124 spectrograph at the Nasmyth secondary focus of the 6 meter Bolshoi Azimutal Telescope, BTA, (Ioannisiani et al. 1982). The spectrograph was equipped with a 1200 lines/mm grating giving a dispersion of 50 Å/mm. A television scanner with two lines of 1024 channels recorded the sky and object spectra simultaneously in a photon-counting mode (Somova et al. 1982; Drabek et al. 1986; Afanasiev et al. 1991).

In March 1996 observations were carried out in a spectropolarimetric mode. In this mode the achromatic analyzer of circular polarization (Najdenov & Panchuk 1996) was installed in front of the slit of the spectrograph and two spectra were recorded in the circular polarizations simultaneously. The sky was observed between the exposures. A 2-arcsecond aperture (in spectral mode) and slit (in spectropolarimetric mode) were used. The spectra in the wavelength passband  $\approx 1000$  Å in the range 3900-5200 Å with a dispersion of 1 Å/channel were obtained with a temporal resolution of 32 ms. The spectra were recorded continuously (1200-5400 s), and between the exposures a He-Ne-Ar lamp was measured for the wavelength calibration. General characteristics and the journal of our observations are presented in Table 1 and Table 2.

**Table 2.** Journal of the observations of RE 0751+14

Date	Filename	Start UT time	Exposure (sec.)	Mode
02/12/93	a3212.01	16:47:39	2860	spectroscopy
02/13/93	a3213.01	16:53:03	4605	
	a3213.02	18:52:58	1523	
	a3213.03	19:26:49	1177	
	a3213.04	19:49:24	4442	
04/02/94	a4402.03	17:57:38	4603	
	a4402.04	19:27:49	2395	
	a4402.05	20:11:34	3329	
04/04/94	a4404.02	17:29:10	5097	
	a4404.03	18:59:25	4661	
03/13/96	a6313.03	18:36:50	4602	spectro- polarimetry
	a6313.05	20:00:26	3607	
03/14/96	a6314.01	17:02:16	3580	
	a6314.02	18:25:00	5400	
03/15/96	a6315.05	18:26:22	5036	
03/16/96	a6316.03	18:40:07	4186	
03/17/96	a6317.02	16:31:30	4390	

### 2.1. Data reduction

The data reduction was performed with the help of a special algorithm. The mathematical justification of the algorithm is given in appendix to the paper. We present here only a short description of this method. As a result of every exposure, a file with the coordinates (2x1024 channels) and the time of registration (resolution 32 ms) for every photoelectron was written on a hard disk in the computer. The possibility of extracting of spectra integrated during the time from 32 ms to the time of exposure (3000-5000 s) from original information (coordinates, 2x1024 channels, and the time of arrival) about photoelectrons with an accuracy limited by the time resolution (32 ms) is the basic idea of our method of data reduction. The range of the investigated periods from 300 s to 2000 s was chosen. This choice makes it possible to analyze the oscillations near the spin period (834 s) and its harmonic and the double period. The resolution along the period was 5 s in the range from 300 s to 600 s, 10 s in the range 600-1200 s and 50 s in the range 1200-2000 s.

For every period (300 s, 305 s, ..., 600 s, 610 s, ..., 1200 s, 1250 s, ..., 2000 s) the spectra with the time of acquisition (30 s, 30.5 s, ..., 60 s, 61 s, ..., 120 s, 125 s, ..., 200 s) were extracted from the original spectral data (the file with the parameters of photoelectrons) and folded in ten bins. Every bin contains two spectra (object and sky or two objects in the polarimetric mode of observations). The number of photons in one bin is equal approximately to the total number of photons in the exposure divided by ten. For every bin, after the subtraction of the sky spectrum (which was strongly smoothed), the continuous spectrum was calculated as a 3d-4th power polynomial and

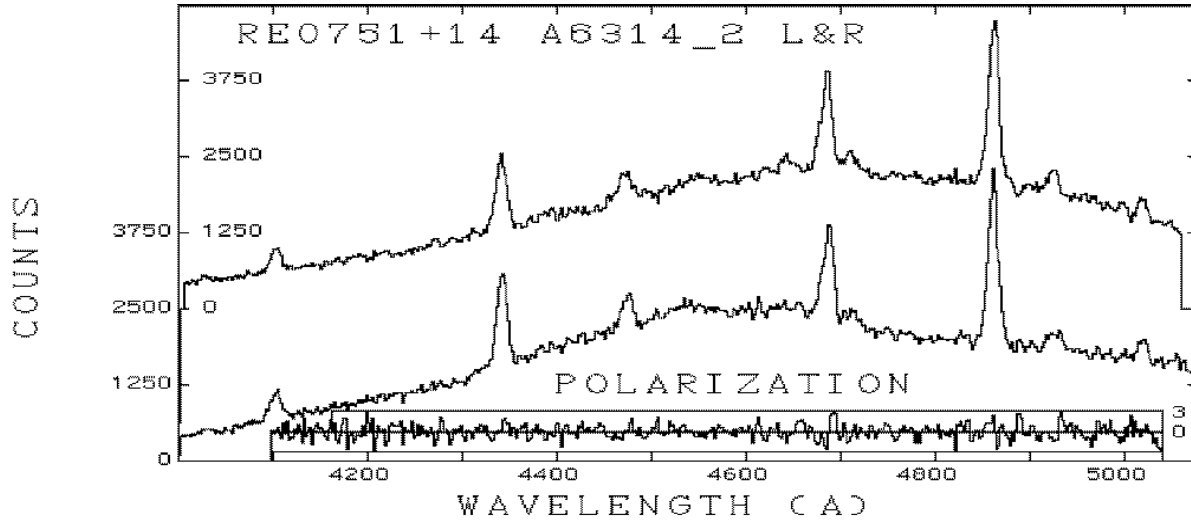


**Fig. 1.** The two simultaneously recorded integral spectra in two circular polarization. The scales of counts are shown inside and outside the frame. The narrow-band variation of polarization in  $\sigma$  units is shown below the spectra

every spectrum was divided by the continuous spectrum. The normalized bin will be

$$R_j(\lambda) = \frac{S_j(\lambda)}{C_j(\lambda)}, \quad (1)$$

where  $j = 1, 2, \dots, 10$  is the number of a bin,  $S_j(\lambda)$  is the spectrum accumulated in one bin,  $C_j(\lambda)$  is the corresponding continuous spectrum,  $R_j(\lambda)$  is the spectrum in one bin in relative units,  $\lambda$  is the wavelength corresponding to the channels.

Further we assume but not underline a discrete character of  $\lambda$ . This conversion to relative units suppresses the broad-band spectral variability (guiding effects, variability of the object itself and spectral window). Then we calculated the power, amplitude and phase of the oscillations in relative units (the level of continuous spectrum is equal to 1) for every channel (wavelength). The Fourier coefficients corresponding to the period of interest were determined as

$$A(\lambda) = \frac{2}{10} \cdot \sum_{j=1}^{10} R_j(\lambda) \cos\left(\frac{2\pi}{10} \cdot j\right), \quad (2)$$

$$B(\lambda) = \frac{2}{10} \cdot \sum_{j=1}^{10} R_j(\lambda) \sin\left(\frac{2\pi}{10} \cdot j\right). \quad (3)$$

The power of the spectral oscillations is equal to

$$|X(\lambda)|^2 = A(\lambda)^2 + B(\lambda)^2, \quad (4)$$

where  $X(\lambda)$  is a complex amplitude of the pulsation.

This method is similar to the method of synchronous detection widely used in astronomical observations. The algorithm was realized in the last version of the special programming language SIPRAN (Somov 1986). The integral spectrum was calculated by simple integration of the photoelectrons. The wavelength calibration (Kopylov et al. 1986) was made with the help

of the He-Ne-Ar lamp. The result of data reduction is the dependence of the power of oscillations on the period (periodogram) and on the wavelength (spectrum), but we will name it a power spectrum for simplicity. In the case of spectropolarimetry as an additional information about circular polarization of the oscillations, the second power spectrum was calculated.

The method was checked by a computer simulation and by observations of standard stars (sun-like star, spectral standard stars without emission lines) and several astrophysical objects such as three intermediate polars and one polar.

To distinguish the difference between our method of observations and data reduction and classical methods we use the word “dynamic” for our case.

### 3. Results. Monochromatic oscillations in the spectrum

Two simultaneously recorded integral spectra of the intermediate polar RE 0751+14 in two circular polarizations are presented in Fig. 1. The spectra show the emission hydrogen lines  $H\beta$ ,  $H\gamma$ ,  $H\delta$ , the helium emission lines HeII 4686, HeI 4471, 4921, 5015 Å, which are typical of intermediate polars. The scale of counts is shown for the lower spectrum beyond the frame. The upper spectrum is shifted and the scale of counts is inside the frame. The circular polarization is presented below the lower spectrum. The vertical scale for the polarization is in  $\sigma$  units, where  $\sigma$  is the root-mean-square deviation from the mean value, which was calibrated, using the results of measurements of the circular polarization in the filter B (Pirola et al. 1993), to zero. The horizontal lines correspond to the mean value of the circular polarization and to  $3\sigma$  deviations.

Significant narrow-band deviations of the circular polarization are not seen in the integral spectra. It is possible to find the date and the time of exposure in the journal of our observations (Table 2), using the file name (A63...) in the figures.

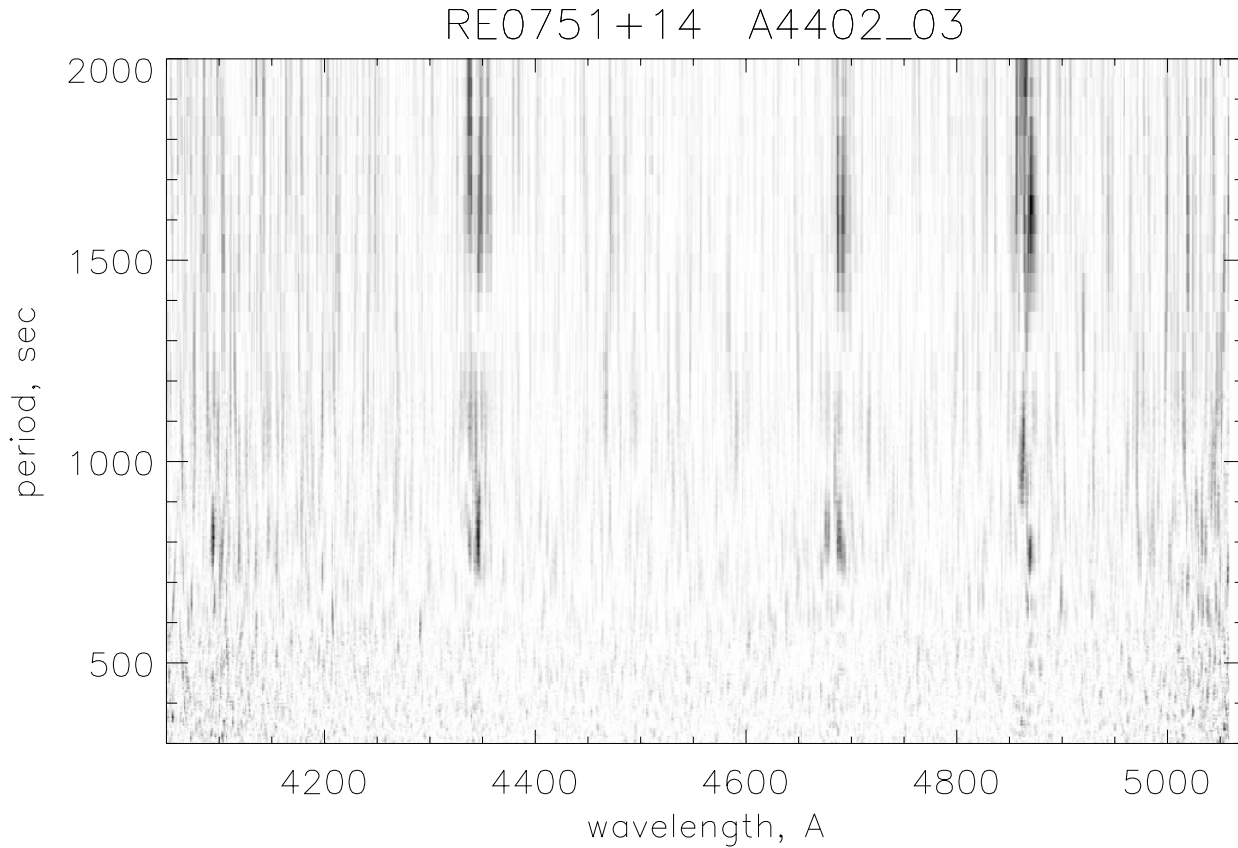


**Fig. 2.** An example of power spectrum as a gray-scale image. The level of gray intensity is proportional to the power of spectral oscillations in arbitrary units

An example of the power spectrum as a gray-scale image calculated by our algorithm of data reduction is illustrated in Fig. 2. The exposure was made on 04/02/1994 in the spectroscopic mode of observations. The level of gray intensity in this image is proportional to the power of spectral oscillations. The horizontal axis presents the wavelength and the vertical axis the period of oscillations. Black narrow bands are seen in this figure at the wavelengths in the profiles of hydrogen emission lines  $H\beta$ ,  $H\gamma$ ,  $H\delta$  and HeII 4686 Å. These black bands point to the increased power of the oscillations in the vicinity of the spin period (834 s) and double period (1700–1800 s). An analysis of this power spectrum has shown that the oscillations in hydrogen lines are not correlated. It means that the wavelengths of the oscillations in hydrogen lines cannot be described by the Doppler effect alone. For example, the signal (we name the features in the power spectra as the signal) in  $H\delta$  is blueshifted at 7 Å, at the same time the signal in  $H\gamma$  is redshifted at 3 Å from the original wavelengths. The signals in  $H\delta$  and  $H\gamma$  have the same period of the maximum of power ( $840 \pm 10$  s), but they are not in phase. The signal in  $H\beta$  is splitted into two components which are separated in wavelengths and periods, and, as a result, it is not possible to compare the signals in  $H\beta$  and  $H\gamma$ .

The first common property of the signals is an independence of the oscillations (the absence of correlation) in the profiles of different emission lines. This property is confirmed by all

our data and means that it is possible to detect signals in all emission lines and to observe oscillations in a single line or in any combination of lines. The absence of oscillations in all lines at all is a rare event but it was also observed.

The second common characteristic of the spectral oscillations is the absence of statistically significant features in the integral spectrum at the wavelengths corresponding to the oscillations. It is true for both the signals inside and outside of the emission line profiles. The fragment of the power spectrum, extracted from the image in Fig. 2, is presented in Fig. 3 in the wavelength region around  $H\delta$ , and in the region of periods in the vicinity of the spin period. The upper spectrum represents the integral spectrum, which has been normalized to the continuous spectrum and is shown in relative units, and all other spectra are power spectra. The power in arbitrary units is along the vertical axis. The wavelength in angstroms is along the horizontal axis. The straight horizontal lines (here and in all the following similar figures) show the level of statistical significance 0.0025 or the probability that the signal is random.

To determine the statistical significance of features in power spectra an individual power spectrum section along wavelength was normalized to mean standard deviation ( $\sigma$ ) from mean value and multiplied by 2. In this case individual power spectrum section has as conventional FFT power spectra (Bonnet-Bidaud et al. 1996), from pure statistics, an expected mean value of

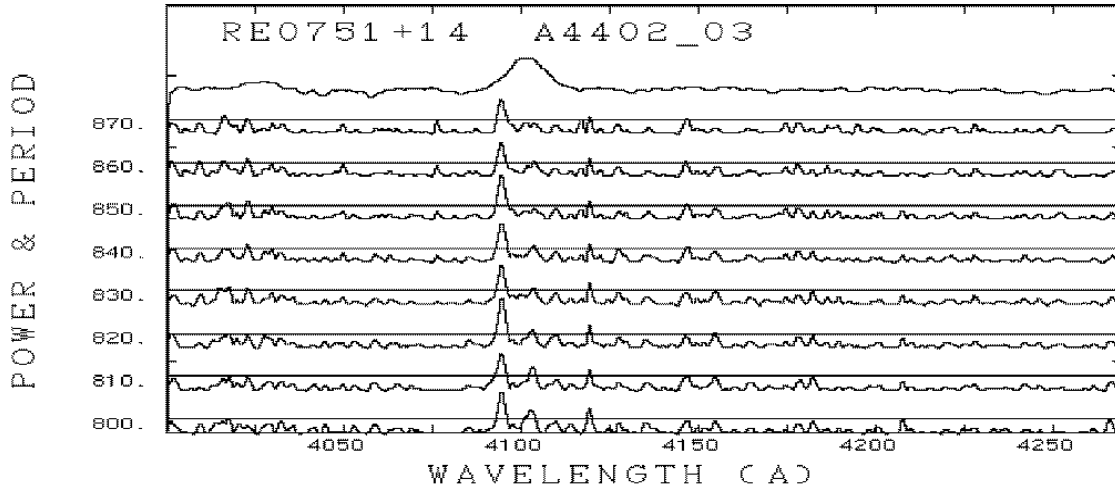


**Fig. 3.** A fragment of the power spectrum extracted from the image in Fig. 2 in the wavelength region near the emission line H $\delta$  and the periods in the vicinity of the spin period. The upper spectrum corresponds to the integral spectrum normalized to the continuous spectrum, and all other spectra are power spectra. The periods are shown in seconds. The scale of power is in arbitrary units along the vertical axis. The straight horizontal lines show the levels of the statistical significance 0.0025 (the probability that the signal is random)

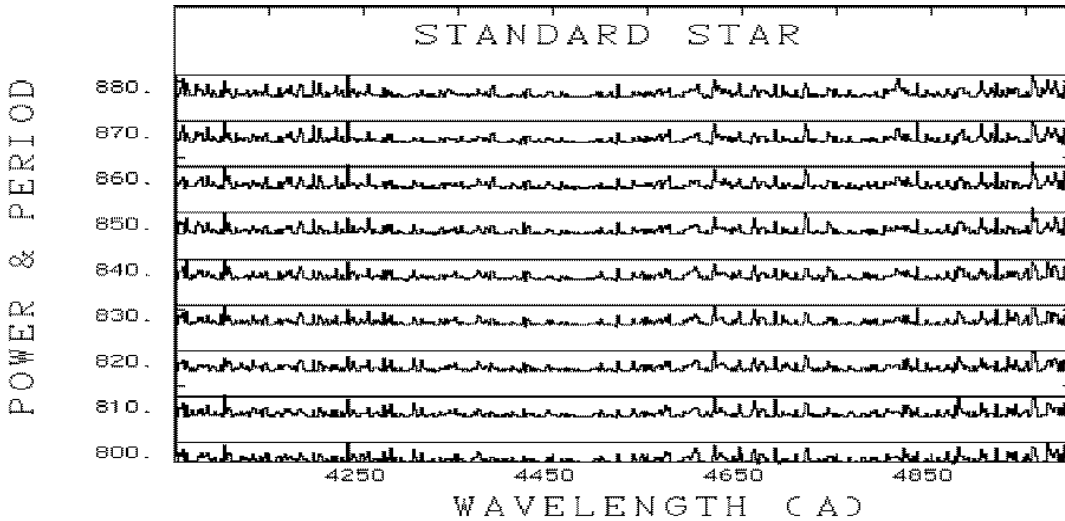


**Fig. 4.** A fragment of the power spectrum of a “standard” star (sun-like star) in the vicinity of the spin period. All spectra are power ones. The periods are shown in seconds. The scale of power is in arbitrary units along the vertical axis. The straight horizontal lines show the levels of the statistical significance 0.0025 (the probability that the signal is random)

2 with mean standard deviation ( $\sigma$ ) of 2 and power values are distributed according to  $\chi^2$  distribution with 2 degrees of freedom (see van der Klis 1989). We assumed that the powers of oscillations in the adjacent channels are independent. The observations of standard stars and the cases of the absence of features in power spectra show that this approximation is satisfactory.

It is seen that the power excess in the blue wing of H $\delta$  does not produce any associated detail in the integral spectrum.

The absence of significant power of the oscillations in the spectrum of a standard star (sun-like star) in the vicinity of the spin period is illustrated in Fig. 4. Similar power spectra without significant features are found in observations of spectral standard stars too.

An example of monochromatic power spectrum (the wavelength passband is equal to 1 Å) in the profile of H $\gamma$ , recorded on February 13, 1993 is shown in Fig. 5. The marks in the upper part of the figure (here and after) demonstrate the periods 415 s ( $2\omega$ ), 830 s ( $\omega$ ), 870 s ( $\omega - \Omega$ ) and 910 s ( $\omega - 2\Omega$ ), where  $\omega$  is the spin frequency and  $\Omega$  is the frequency of the orbital period.

There are two features in the power spectrum with maxima at the periods 900 s and 440 s. The amplitude of the oscillations at the period 900 s was 30%. The signal-to-noise ratio was equal to 28. The statistical significance or the probability that the signal is random is equal to  $10^{-12}$ . This is an example of detection of the monochromatic spectral oscillations in the wavelength passband 1 Å in the observations of 1993. The possibility of

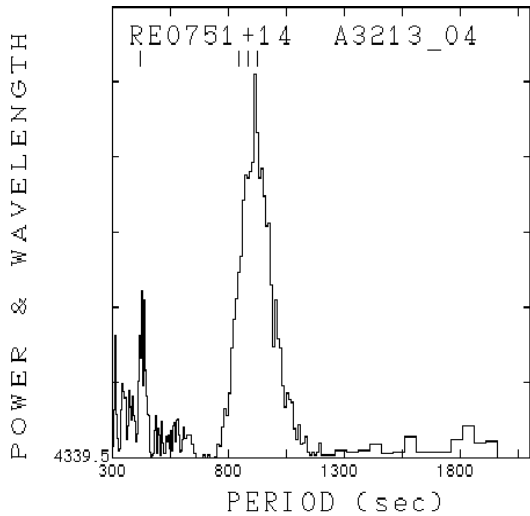


**Fig. 5.** An example of a monochromatic power spectrum (the wavelength passband is equal to  $1 \text{ \AA}$ ) in the profile of the emission line  $H\gamma$  recorded on February 13, 1993. The scale of power is in arbitrary units along the vertical axis. The marks in the upper part of the figure and in all similar ones correspond to the frequencies  $2\omega, \omega, \omega - \Omega, \omega - 2\Omega$ , where  $\omega$  and  $\Omega$  are the spin and orbital frequencies respectively

concentration of the oscillations in the narrow (FWHM in the power spectrum is  $2-3 \text{ \AA}$ ) wavelength passband in the profiles of emission lines was not predicted by any model of optical oscillations, and this property is unexpected.

In spite of the absence of polarization effects in the broad wavelength band (filter B), the objective of our observations in March 1996 was investigation of circular polarization characteristics of the spectral oscillations, this meant that the classical polarization in the integral spectra would not be measured except for narrow-band fluctuations of circular polarization, which were absent (Fig. 1). Our interest was to investigate the behaviour of spectral oscillations in two circular polarizations.

An example of two simultaneously recorded integral spectra in two circular polarizations was already shown in Fig. 1. The monochromatic power spectra of the blue wing of the  $HeII$   $4686 \text{ \AA}$  emission line in the left (L) and right (R) circular polarizations are presented in Figs. 6a,b. All scales in both figures are equal. Comparison of these figures shows that the oscillations in the vicinity of the spin period dominated in the right circular polarization. In addition, Fig. 6a illustrates a relatively broad-band (the width up to  $\approx 10 \text{ \AA}$ ) oscillations. In a general case the oscillations can be presented by two components: relatively broad and very narrow (FWHM in the power spectrum is  $2-3 \text{ \AA}$ ). The probability of detection of the broad component is lower than of the narrow one.

The monochromatic power spectra were extracted from this exposure at the wavelength  $4680 \text{ \AA}$  and are shown in Figs. 7a,b on greater scale of power. For comparison, the monochromatic power spectra from the same exposure, but in the blue wing of the emission line  $H\beta$  at the wavelength  $4852.8 \text{ \AA}$  in the red wing of the emission line  $H\gamma$  at the wavelength  $4344 \text{ \AA}$  in the

profile of the emission line  $H\delta$  at the wavelength  $4101 \text{ \AA}$  are demonstrated in Figs. 8a,b, 9a,b, 10a,b. In all Figs. 6-11,13 the left figure correspond to the left and the right one to the right circular polarization. The scale of power is in arbitrary units and in Figs. 10a,b the scale is duplicated in comparison to Figs. 7a,b. It means that the amplitude of the oscillations in  $H\delta$  was greater than in  $H\beta$ . The marks in the upper part of the figures correspond to the frequencies  $2\omega, \omega, \omega - \Omega, \omega - 2\Omega$ , where  $\omega$  and  $\Omega$  are the spin and orbital frequencies respectively

The oscillations are readily seen to be strongly polarized. We introduce a formal measure of dynamic polarization  $P_d$  which will characterize the observed oscillations as

$$P_d = \frac{P_l - P_r}{P_l + P_r} \cdot 100\%, \quad (5)$$

where  $P_l$  and  $P_r$  are the powers of the oscillations in the left and right polarizations at the same period and at the same wavelength. This formal measure of polarization for the wavelength  $4852.8 \text{ \AA}$  is equal to  $90\%$  and for the wavelength  $4680 \text{ \AA}$  it is equal to  $-90\%$ . It should be noted that the sign of the dynamic polarization in  $H\gamma$  was opposite to that of  $H\beta$  in this exposure. This is an additional argument for the independence of the spectral oscillations in the profiles of different emission lines.

Comparison of the periods of the maxima of power in the left and right polarizations shows the symmetrical shifts relative to or from the spin period. If  $\omega$  is the spin frequency and  $\Omega$  is the orbital frequency (the period  $\sim 5.3$  hours), then the periods of the maxima of power in the circular polarizations correspond to  $\omega - \Omega$  and  $\omega + \Omega$ . The symmetrical splitting of the maximum power periods of the signals in the different circular polarizations is a often observed feature of the oscillations at close wavelengths. The splitting of the periods of the maxima of power in rare cases of detection of the signals at the same wavelength in two polarizations was observed too.

The features in the power spectra, which were beyond the profiles of the known emission lines, were also detected. An example of one of this kind of features, blueshifted from  $H\gamma$ , at the wavelengths around  $4190 \text{ \AA}$  is shown in Figs. 11a,b. Another example, blueshifted from  $H\delta$ , at the wavelength  $4039 \text{ \AA}$  is shown in Fig. 12. This figure demonstrates also the case of the absence of the oscillations in  $H\gamma$ , while the oscillations exist in  $H\delta$ . It means that there is no direct correlation between the number of photoelectrons (see Fig. 1) and the oscillations either.

The monochromatic power spectra for the wavelength  $4039 \text{ \AA}$  in the left and right polarizations are shown in Fig. 13a,b. The signal-to-noise ratio for this feature is lower than for the features in the profiles of the emission lines, but the polarized signal is seen clearly.

The principal parameters of the narrow-band spectral oscillations are presented in Table 3. For all parameters we give the region of variations, because the detected spectral oscillations cannot be described as stable periodical pulsations. These oscillations have to be assigned to quasi-periodical ones with all parameters varying with time. The time of life or the time of coherence of the monochromatic oscillations is about the time

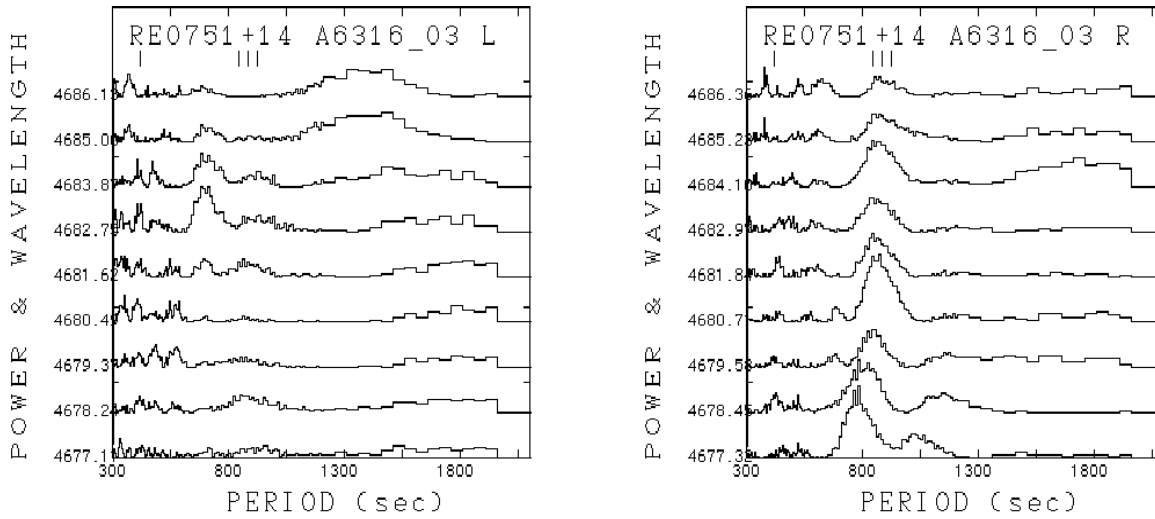


Fig. 6. a,b Monochromatic power spectra in the blue wing of the HeII 4686 Å emission line

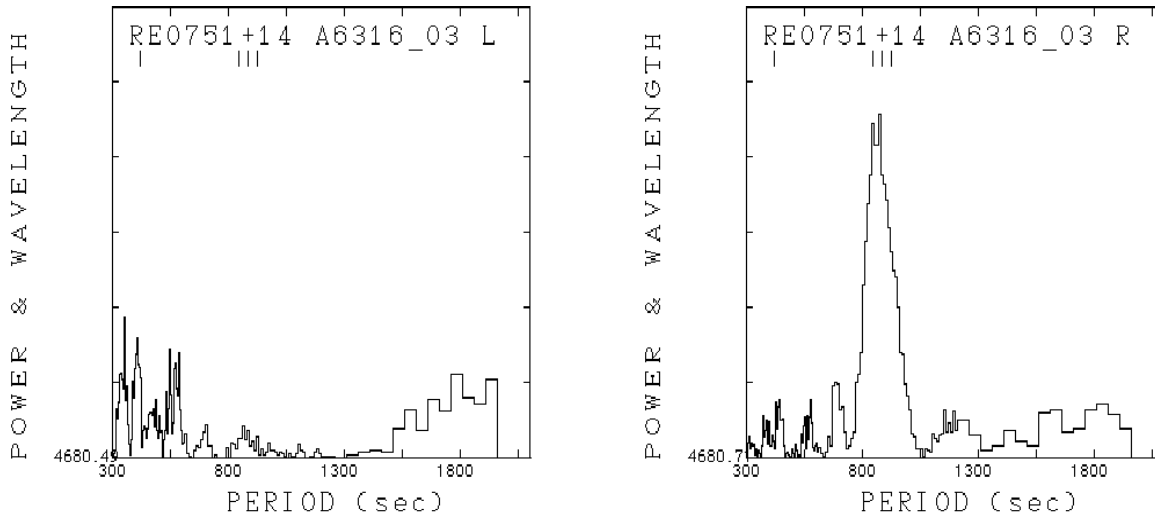


Fig. 7. a,b The monochromatic power spectra on an increased scale of power at the wavelength 4680 Å

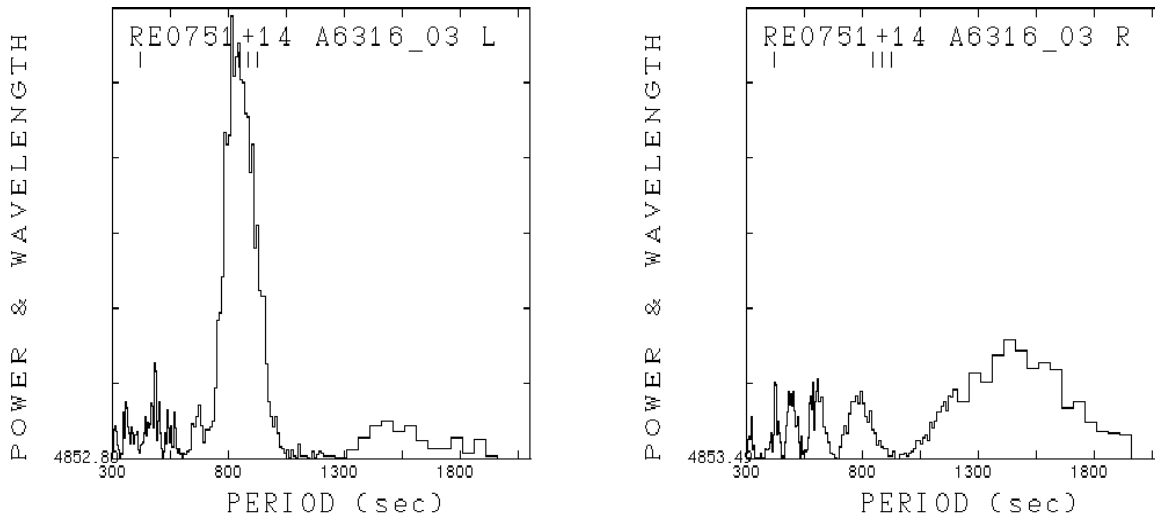
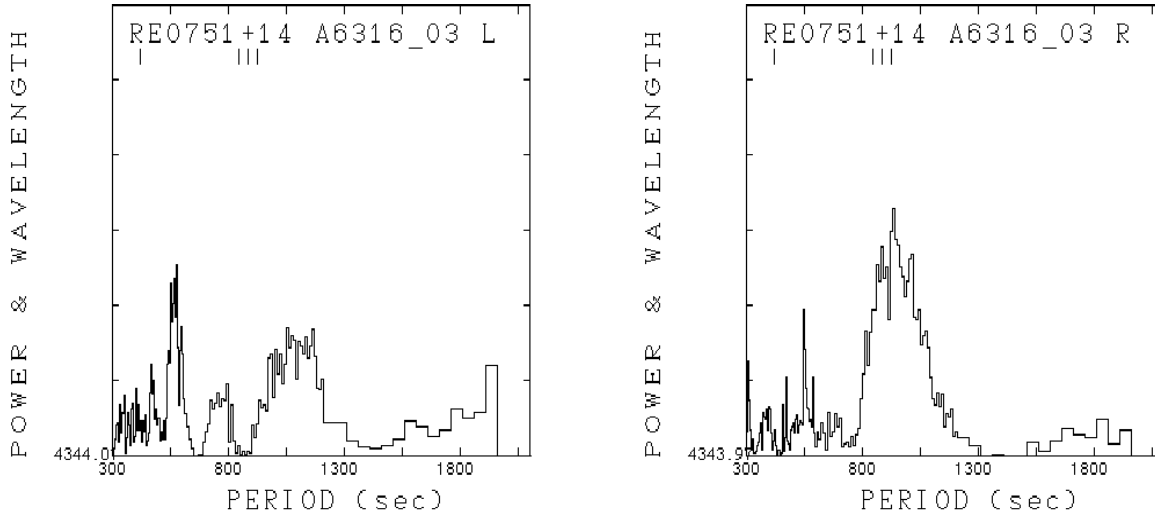
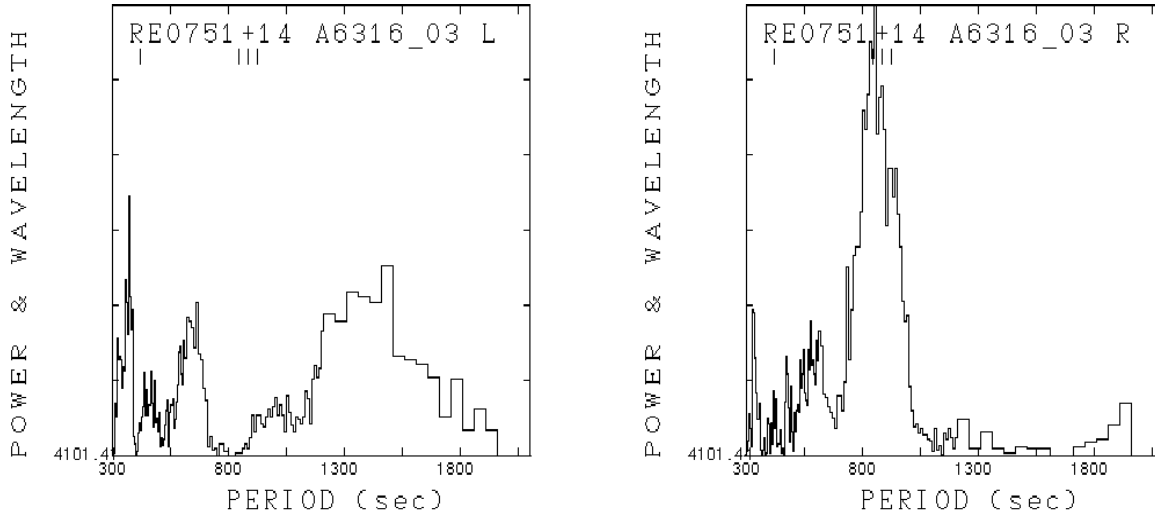


Fig. 8. a,b The monochromatic power spectra on the same, as in Fig. 7a and b scale of power at the wavelength 4853 Å



**Fig. 9. a,b** The monochromatic power spectra on the same, as in Fig. 7a and b scale of power at the wavelength 4344 Å



**Fig. 10. a,b** The monochromatic power spectra at the wavelength 4101 Å

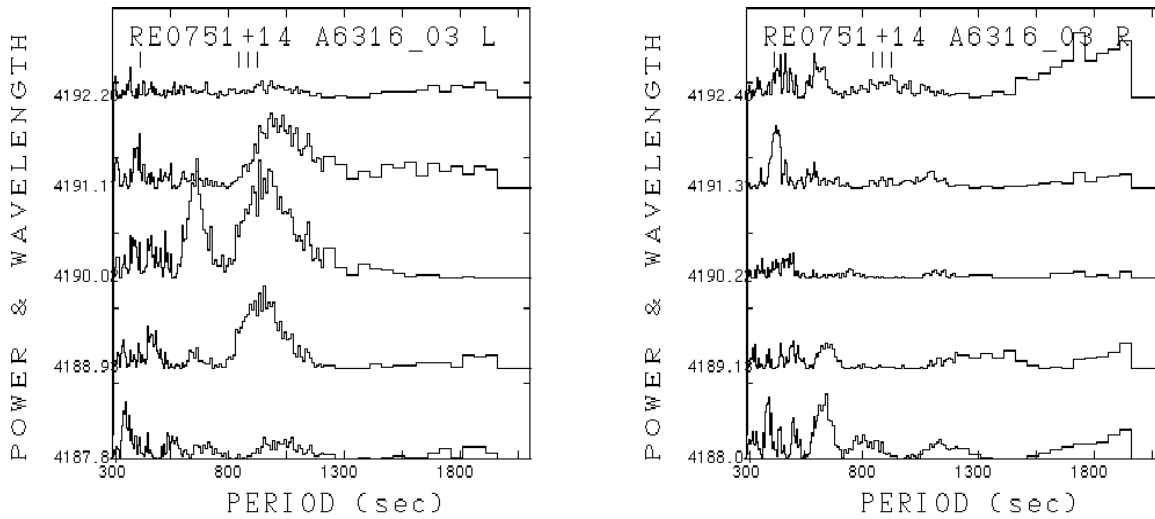


**Fig. 11. a,b** Monochromatic power spectra in the wavelength range outside of profiles of emission lines

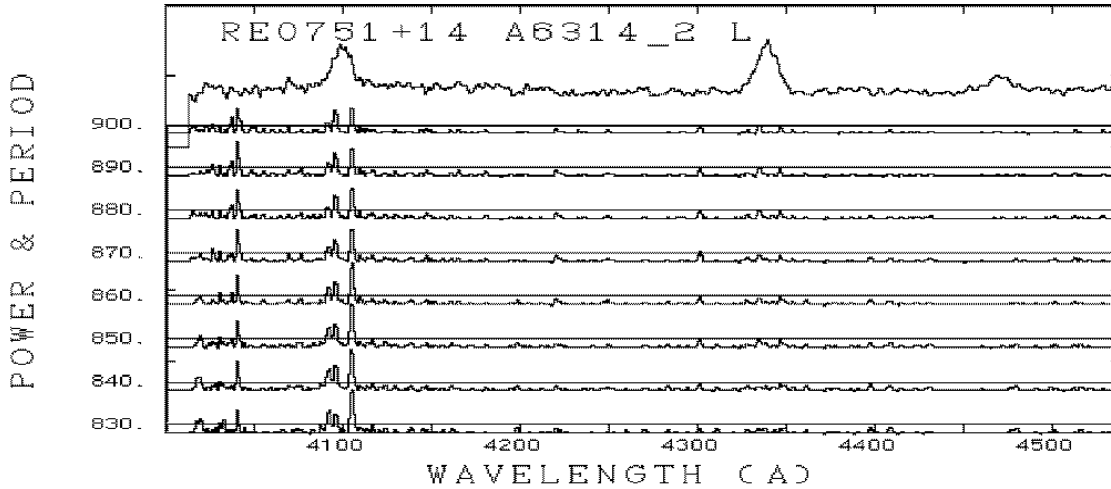


**Fig. 12.** A fragment of power spectrum in the left circular polarization in the wavelength region near the emission line H $\delta$  and the periods in the vicinity of the spin period. The upper spectrum corresponds to the integral spectrum normalized to the continuous spectrum, and all other spectra are the power spectra. The periods are shown in seconds. The scale of power is in arbitrary units along the vertical axis. The straight horizontal lines show the levels of the statistical significance 0.0025 (the probability that the signal is random). The feature at the wavelength 4039 Å is readily seen

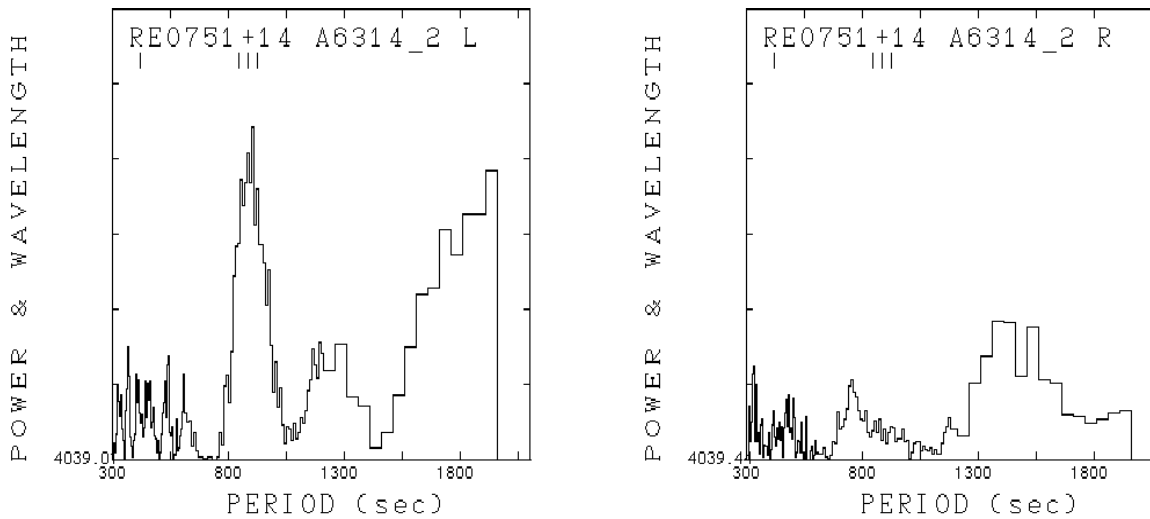


**Fig. 13. a,b** The monochromatic power spectra on an increased scale of power at the wavelength 4039 Å

of exposure and equals about 3000-5000 s. It means that the signals in neighbouring exposures were detected but with different parameters (wavelength, period, amplitude, polarization). An attempt to calculate the power spectra from the combination of several exposures has shown that the time of life of the monochromatic oscillations is limited.

In addition to the known pulsations over the spin period of the light curves in photometric observations and variations of the V/R ratio of emission lines in spectral observations at other telescopes we have presented the detection of the monochromatic oscillations in the wavelength passband 1 Å.

#### 4. Discussion

Some intermediate polars display emission-line profile variations over the spin period (Patterson 1994; Penning 1985; Helier et al. 1987, 1990, 1991; Buckley & Tuohy 1989, 1990). Helier and Mason (1990) reviewed the literature and concluded that in most cases an emission line represented “accretion-column” emission. However, the result on DQ Her suggested that the emission lines indicate a motion in the disk rather than in the column (Chanan et al. 1978; Martell et al. 1995; Patterson 1994). The simplest but strong model which can explain the spectral oscillations in the wings of the emission lines is the periodical motion of the emission line along the wavelength due to the Doppler effect. This means that the periodical motion or period-

**Table 3.** Parameters of the narrow-band spectral oscillations

Parameter	Value	Comments
period	13.3-15.2 min	(1)
amplitude	0-40%	(2)
narrow features FWHM(Å)	2-3 Å	(3)
broad features WIDTH (Å)	6-10 Å	
dynamic circular polarization	60-90%	(4)
wavelengths	mainly in the profiles of the emission lines	(5)
probability that individual detection of the signal is random	$10^{-10} - 10^{-13}$	

Comments:

- (1) the harmonic and the double period also are observable
- (2) the mean noise amplitude was 4-8%, zero means the absence of detectable oscillations
- (3) broad features were observed more rarely than narrow
- (4) the measure of polarization is  $(P_l - P_r)/(P_l + P_r) \cdot 100\%$ , where  $P_l, P_r$  are the powers in the left and right polarizations at the same period and the same wavelength
- (5) more rarely the oscillations were seen out of the profiles of the emission lines

ical perturbation produced by the “hot spot”, running along the inner surface of the accretion disk, can cause the spectral oscillations in the profiles of the emission lines. In our case this model meets serious problems in our observational data. First of all there is the possibility of concentration of the oscillations in the narrow wavelength passband and the strong dynamic circular polarization of the oscillations, and the independent behaviour of the oscillations in hydrogen lines. All these properties cannot be explained by the Doppler effect alone.

We begin to search for an explanation of the detected spectral oscillations in the “accretion-column” radiation from the strong magnetic field.

#### 4.1. Period of the oscillations

In the frame of a standard model of intermediate polars (Patterson 1994) such as an oblique magnetic rotator, we consider the intensity of radiation of a point source (one atom of hydrogen, for example, and, of course, this is an abstraction) situated in the accretion column in the strong magnetic field. We define the orthogonal system of coordinates (XYZ). The Z-axis is aligned with the axis of rotation (the frequency is  $\omega$ ) of the white dwarf, the X-axis, the line of sight and the Z-axis are in one plane. Let the angle between the vector of the magnetic field  $\mathbf{H}$ , which is directed along the accretion column, and the Z-axis be  $\theta$ , and the angle between the line of sight and Z-axis be  $i$ . The wavelengths

of radiation of our point source will be splitted according to the Zeeman effect. The angular distribution of intensity of radiation of the  $\sigma$  components is proportional to  $(1 + \cos^2(\gamma))$  and for the  $\pi$  components to  $\sin^2(\gamma)$ , respectively, where  $\gamma$  is the angle between the vector of the magnetic field and the line of sight. The vector  $\mathbf{H}$  rotates around the Z-axis with an angular velocity  $\omega$  and the  $\cos(\gamma)$  is equal to

$$\cos(\gamma) = \sin(\theta) \cdot \sin(i) \cdot \cos(\omega t) + \cos(\theta) \cdot \cos(i), \quad (6)$$

and  $\cos^2(\gamma)$  is

$$\cos^2(\gamma) = A \cos(\omega t) + B \cos(2\omega t) + C, \quad (7)$$

where

$$\begin{aligned} A &= 0.5 \sin(2\theta) \sin(2i) \\ B &= 0.5 \sin^2(\theta) \sin^2(i) \\ C &= \cos^2(\theta) \cos^2(i) + 0.5 \sin^2(\theta) \sin^2(i). \end{aligned} \quad (8)$$

The intensity  $I$  of radiation of the  $\sigma$  components of the point source will vary in time as

$$I = I_0 \cdot (1 + C + A \cos(\omega t) + B \cos(2\omega t)), \quad (9)$$

where  $I_0$  is a constant. From Eq. (9), it is seen that regular rotation of the accretion column and hence the axis of the magnetic field leads to modulation of the intensity of radiation of the  $\sigma$  components (and  $\pi$  components also) of any point source of radiation in the accretion column. The modulation will be bi-harmonic ( $\omega$  and  $2\omega$ ) and the amplitudes will depend on the geometry ( $\theta$  and  $i$ ). From (8) the ratio of the amplitudes can be written as

$$\frac{B}{A} = 0.25 \tan(\theta) \tan(i). \quad (10)$$

The small perturbation of the regular rotation can also be considered. For example, the angle  $\theta$  varies periodically (a nutation of accretion column) with the frequency  $\Omega$  which is less or much less than  $\omega$ . In this case the coefficients  $A, B, C$  are the functions of time, which can be presented as

$$\begin{aligned} A(t) &= A_0 + A_1 \cos(\Omega t + \Phi_{a1}) + A_2 \cos(2\Omega t + \Phi_{a2}) + \dots \\ B(t) &= B_0 + B_1 \cos(\Omega t + \Phi_{b1}) + B_2 \cos(2\Omega t + \Phi_{b2}) + \dots \\ C(t) &= C_0 + C_1 \cos(\Omega t + \Phi_{c1}) + C_2 \cos(2\Omega t + \Phi_{c2}) + \dots, \end{aligned} \quad (11)$$

where  $\Omega$  is the frequency of nutation and  $\Phi$  are the associated phases. If we substitute (11) in (9) then the appearance of the modulation at side-band frequencies ( $\omega \pm n\Omega$ ) and ( $2\omega \pm n\Omega$ ) will be evident.

So, we can conclude that the intensity of radiation of any point source (one atom) in the accretion column will be modulated over the period of rotation (and over the period of the first harmonic) of the white dwarf at the corresponding wavelengths.

#### 4.2. Wavelength of the oscillations

The wavelengths of radiation of our point source is determined by the value of the magnetic field (Zeeman effect) and by the velocity (Doppler effect). We suppose that the Doppler effect is small and consider the Zeeman effect alone. This assumption is true if the source of radiation is close to the surface of the white dwarf. In the weak magnetic field we have to observe a normal Zeeman triplet, which is missing in our data (power spectra), it means that it is necessary to consider the variant of a strong magnetic field in which the quadratic Zeeman effect must be taken into account. We base our consideration of the Zeeman effect (only for hydrogen lines) on the computations of this effect by Kemic (1974). According to his calculations, the normal Zeeman triplet in the strong magnetic field ( $B > 3$  MGs) is splitted into multitude of components. With an increasing of the strength of magnetic field the  $\sigma-$  and  $\pi$  components are always blueshifted and only the  $\sigma+$  components regain the original wavelength in the profile of the corresponding emission line, when the quadratic wavelength blueshift is equal to the linear wavelength redshift. Our supposition is that the source of radiation which produces the monochromatic spectral oscillations is located in this strong peculiar magnetic field. In other words, we assume that the magnetic fields, when the  $\sigma+$  component regains its original wavelength, are peculiar or resonance. The observational arguments in favour of this fact are as follows. The strongest spectral oscillations were detected in the profiles of the emission lines and strong dynamic circular polarization of these oscillations was observed. The last crucial argument to support our assumption is detection of the  $\sigma-$  components to measure this resonance magnetic field directly.

In the resonance magnetic field (this is our definition) the difference in energy between the high and the low quantum level is equal to this difference in the zero magnetic field for  $\sigma+$  transitions

$$\Delta E_{\sigma+} = E_n - E_m, \quad (12)$$

where  $E_n, E_m$  are eigenvalues of the unperturbed hamiltonian.

For the  $\sigma-$  transitions it is

$$\Delta E_{\sigma-} = E_n - E_m + 2\hbar\omega_l, \quad (13)$$

where

$$\omega_l = \frac{eB}{2mc} \quad (14)$$

is the Larmor frequency. The additional magnetic energy  $2\hbar\omega_l$  coincides with the energy of the cyclotron transitions of free electrons in the same magnetic field.

For  $\pi$  transitions it is

$$\Delta E_{\pi} = E_n - E_m + \hbar\omega_l, \quad (15)$$

where the following relationship was used

$$\hbar\omega_l = \mu_b \cdot B, \quad (16)$$

where  $B$  is the magnetic field and  $\mu_b$  is the Bohr magneton.

We do not try to provide a theoretical support of this peculiarity for the moment, because the nature of the oscillations is not clear and we simply check our supposition. For this it is necessary to calculate the resonance magnetic fields and the wavelengths of the  $\sigma-$  components in the fields.

These calculations have been made on the basis of the tables of Kemic (1974) in the following way. According to Kemic, the contribution to the hamiltonian of an atomic electron due to an external magnetic field magnitude  $B$  is

$$\hat{H}_m = \frac{eB}{2mc} \hat{L}_z + \frac{e^2}{8mc^2} B^2 r^2 \sin^2(\theta), \quad (17)$$

where  $\hat{L}_z$  is the operator for the component of angular momentum along the field,  $r$  and  $\theta$  are usual polar coordinates in a system, whose polar axis is taken along  $B$ .

We have already designated the Larmor frequency as  $\omega_l$  and write the split of the quantum level in the magnetic field as

$$E = E_n + M \cdot \hbar\omega_l + \alpha \left( \frac{1}{2} m \omega_l^2 R_n^2 \right), \quad (18)$$

where  $M = -n, -n+1, \dots, n$  is the projection of the full mechanic momentum on the axis of the magnetic field,

$E_n$  - the energy of the main unperturbed state,

$m$  - the mass of the electron,

$R_n$  - Bohr radius, corresponding to the main quantum number  $n$ ,

$\alpha$  - the coefficient depending on all quantum numbers, and to define this number we have put the similar coefficient for the low level equal to one and calculated  $\alpha$  for the high level with the help of the Kemic tables.

For  $H\delta$  transitions the calibration magnetic field is 3 MGs in which  $\alpha$  is determined, then it is easy to calculate the value of the resonance magnetic field and extrapolate energetic levels to this field and compute the wavelength of the transition. For the strogest  $\sigma-$  transition of  $H\delta$  this extrapolation was done from 3 MGs to 4 MGs, the same was done for  $H\gamma$  from 10 MGs to 9 MGs. The accuracy of our calculations of the wavelength in the calibration magnetic field was 0.1 Å (a fitting to the table value). The value of the resonance magnetic field was determined from the equation for the high level

$$\hbar\omega_l = \alpha \left( \frac{1}{2} m \omega_l^2 R_n^2 \right). \quad (19)$$

For the transitions in  $H\delta$  and  $H\gamma$  the quadratic effect for the low level was not taken into account, but for  $H\beta$  it becomes significant and it is necessary to allow for the quadratic effect for the low level and calculate the resonance magnetic field from the equation

$$\hbar\omega_l = \alpha_1 \left( \frac{1}{2} m \omega_l^2 R_n^2 \right) - \alpha_2 \left( \frac{1}{2} m \omega_l^2 R_m^2 \right), \quad (20)$$

where  $\alpha_1$  and  $\alpha_2$  must be found for each level. Of course, these calculations can be made correctly only by the quantum mechanics methods. The results of our computations and the observations only for the strongest  $\sigma-$  transitions for  $H\delta$  and  $H\gamma$

**Table 4.** The wavelengths of the strongest  $\sigma-$  transitions of the hydrogen lines H $\delta$  and H $\gamma$  in the resonance magnetic fields

transition	resonance magnetic field (MGs)	wavelength	
		computation	observation
2p1 => 6d2	3.9	4039.80(1)	4039.2(2)
2p1 => 5d2	9.0	4188.61(1)	4189.7(2)

are shown in Table 4. The maximal possible errors in angstroms are presented in brackets (the accuracy of the Kemic tables for the calibration fields is better than 1 Å). For the  $\sigma+$  components the difference between the calculations and the observations can be  $\pm 10$  Å (the whole profile of the emission line). It should be noted that the values of the resonance magnetic fields for different transitions are significantly different.

The presence of the signals at the calculated wavelengths for the strongest  $\sigma-$  transitions for the hydrogen lines H $\delta$ , H $\gamma$  and H $\beta$  was checked in our data. The examples of the H $\delta$   $\sigma-$  signal is shown in Figs. 12, 13a,b and of the H $\gamma$  in Figs. 11a,b. We could not find the  $\sigma-$  signal of H $\beta$  in all our data.

The simplest explanation is that the magnetic moment (the electron orbit) prefers to be aligned with the magnetic field. In this case the energy of the magnetic momentum is lower than in the opposite orientation. The strongest  $\sigma+$  transitions correspond to the orientation of the magnetic momentum of the orbit along the magnetic field (the negative sign of the projection of the mechanical moment). One can check this in the same Kemic tables. For the strongest  $\sigma-$  transitions the situation is opposite. The orientation of an electron orbit in a very strong magnetic field (for H $\beta$  the resonance magnetic field is  $\sim 26$  MGs) is expected to be polarized, and, consequently, observations of the  $\sigma-$  transitions will be problematic.

The calibration of this resonance effect was possible only for the H $\delta$  and H $\gamma$   $\sigma-$  components in our data. The assumption of resonance or peculiar magnetic fields is consistent with the solutions of the Schrödinger equation in the strong resonance magnetic fields, at least, for the strongest  $\sigma-$  transitions of the hydrogen lines H $\delta$  and H $\gamma$ .

On the basis of this empirical fact it can be concluded that the sources of the spectral oscillations are really in the strong resonance magnetic fields (for H $\delta$   $\approx 4$  MGs, for H $\gamma$   $\approx 9$  MGs, for H $\beta$   $\approx 26$  MGs, for HeII 4686 Å  $\gtrsim 100$  MGs).

#### 4.3. The nature of radiation from the strong magnetic field

The idea that the source of the monochromatic spectral oscillations is in the strong magnetic field can explain the basic characteristics of the spectral oscillations such as the period of oscillations, the wavelength of oscillations, the circular polarization, the independent behaviour of the signals in the profiles of different emission lines because they come from different resonance magnetic fields and, consequently, from different parts of the accretion column.

Now we have to explain the last common property of the oscillations, which is the absence of any significant narrow details in the integral spectrum at the corresponding wavelengths. First of all we try to understand what the source of spectral oscillations radiates.

There are the following alternatives:

1. The source emits photons. In this case the integration of photoelectrons must reveal the feature in the integral spectrum, which is associated with the oscillations and which is not seen in our data. So, we must reject this variant.
2. The source absorbs photons. The integration of photoelectrons must also reveal the feature in the integral spectrum. It is also missing in our data, and we must abandon this variant.
3. The source emits and absorbs photons in an exactly periodical way. The source can be imagined to be a photon emitter, however, it is impossible to account for the absorption of the 40% of photons in a hydrogen line profile as due to the compact source (the size of the source is severely restricted by the accretion column and the resonance magnetic field). This alternative should be dropped too.

It should be noted that the Doppler effect (the periodical motion of the whole emission line along the wavelength) does not cause any narrow features in the integral spectrum. Neither can the effect produce polarization and noncorrelation in the behaviour of oscillations in hydrogen lines.

We formulate our principal observational result only as discovery of a signal as the strong statistically significant perturbation of spectral composition of photoelectron noise in the narrow wavelength passband (1 Å) in the close vicinity of the spin period, mainly in profiles of emission lines. Based on our observations and this simple consideration of alternatives a conclusion can be drawn that no reasonable interpretation in frame of ordinary physics of the monochromatic spectral oscillations as the monochromatic oscillations of the photon flux is available as yet. It means that a standard way of thinking that statistically significant oscillations of the monochromatic photoelectron flux reflect the associated variations of the photon flux, leads to great problems with a common sense in frame of conventional physics and from our point of view has no perspectives.

In this situation we propose, as an hypothesis or if one wants a speculation, to invoke for an explanation our observations instead of classical photons electromagnetic waves with parallel electric and magnetic vectors or the Pointing vector equal to zero which should be considered as a physical counterpart of the waves of probability in quantum mechanics. This kind of electromagnetic waves cannot transmit an energy but can produce additional perturbation for an electron in the photocathode and it can lead to local periodical variations of the quantum efficiency of the photocathode. The wave has to be monochromatic and coherent. It is interesting to note that an acceptance of a physical reality of this kind of waves leads to the "hairs" of black holes and in this case the source of strong radiation of this kind of electromagnetic waves can be a black hole.

**Table 5.** Comparison of parameters of the photometric (filter B) and monochromatic oscillations for RE 0751+14

Parameter	broad band (filter B)	Ref.	narrow band (1 Å)
Period	13.9-14.5 min	(1)	13.3-15.2 min
Amplitude	0-8%	(1)	0-40%
Polarization	in B filter=0%	(2)	60-90% (dynamic)
Magnetic field	8-18 MGs	(2)	4-9 MGs

(1) Hellier et al. 1994

(2) Piirola et al. 1993

#### 4.4. Comparison with other observations

In the previous consideration we have shown that the monochromatic oscillations give us an information about the object and here our results will be compared with the photometric observations at other telescopes. The parameters of the photometric and monochromatic oscillations are presented for a comparison in Table 5.

It is seen from the Table 5 that periods corresponding to the maxima of power of the monochromatic oscillations are in a vicinity of the known spin period. The vicinity corresponds to a range of frequencies from  $\omega - 2\Omega$  till  $\omega + \Omega$ , where the oscillations in light curves (filter B) in this range of frequencies were observed in many intermediate polars (Patterson 1994). It means that the period of the monochromatic oscillations gives us an information about the spin period and can be used at least for estimations of the spin period of the white dwarf.

A comparison of amplitudes of oscillations shows that the amplitudes of monochromatic oscillations can be significantly greater than photometric ones.

The absence of circular polarization in filter B is compatible with the absence of significant narrow band deviations of polarization in the integral spectra (Fig. 1). The strong dynamic polarization of oscillations should be considered only as an indication to a nonthermal mechanism of radiation causing the oscillations.

The estimation of magnetic field derived from the UBVR polarization measurements is compatible with our measurements of magnetic field by means of the detection of the oscillations at the wavelengths corresponding to the strongest  $\sigma$ -transitions of H $\delta$  and H $\gamma$  in the computed resonance magnetic fields.

The independent spectral observations (Rosen et al. 1993) have revealed the oscillations of the ratio V/R and radial velocity in the emission lines in the same wavelength region. It is evident, that the presence of the strong narrow-band oscillations in the wing of the emission line (for example, see Fig. 8a) can and produces the oscillations of the ratio V/R and the radial velocity. We have checked this in our data and observed direct correlation between the presence of the monochromatic oscillations in the profile and oscillations of the parameters of emission line.

The detection of the oscillations outside of the profiles of emission lines has no known analogs for a comparison.

The comparison of our and other observations shows that our conclusions are consistent with other ones and can be considered as the additional evidence for the available information about RE 0751+14. Nevertheless we do not know and believe that it does not exist a reasonable explanation of the discovered monochromatic oscillations in frame of a conventional physics.

## 5. Conclusion

We have presented the first results of optical dynamic spectroscopy and spectropolarimetry of the intermediate polar RE 0751+14 obtained with help of scanner BTA in high time resolution mode at the 6 m telescope from February 1993 till March 1996. The statistically significant perturbations of spectral composition of photoelectron noise in the narrow wavelength passbands (1 Å) were detected in power spectra. The strong (amplitude till 40%), polarized (dominating in one polarization), monochromatic (FWHM in power spectra 2-3 Å) oscillations at the periods 13.3-15.2 min have been discovered with the help of special algorithm.

The wavelengths of the oscillations correspond to the solutions of the Schrödinger equation in strong resonance magnetic fields (quadratic Zeeman effect). The equation for calculations of the resonance magnetic fields for  $\sigma$  transitions is the equality of the wavelength shifts due to the linear and quadratic terms of the Zeeman effect.

We conclude that the sources of radiation causing the spectral oscillations are in the accretion column of the white dwarf in the strong resonance magnetic fields equal for H $\delta$   $\approx$ 4 MGs, for H $\gamma$   $\approx$ 9 MGs, for H $\beta$   $\approx$ 26 MGs.

However we do not know and believe that it does not exist a reasonable explanation of the discovered monochromatic oscillations in frame of a conventional physics.

*Acknowledgements.* We are grateful to:

Prof. I.M. Kopylov for support of our direction of investigations and helpful discussions;

Drs. J.M. Bonnet-Bidaud and M. Mouchet for initiating and support of our investigations of RE 0751+14 ;

Prof. Yu.Yu. Balega and V.L. Afanasiev for reading the manuscript and helpful discussions;

Dr. Carol Adams for support of our investigations and interesting discussions.

## Appendix A: mathematic justification of algorithm

A result of the spectral observations with the BTA scanner in a high time resolution mode is a file with the coordinates (2x1024 channels) and the time of detection (resolution 32 ms) for every photoelectron, which was recorded during one exposure. Every channel corresponds to the wavelength and can be calibrated with the help of a He-Ne-Ar lamp spectrum. The flux of photoelectrons is described by the function  $F(\lambda, t)$ , where  $\lambda$  is the wavelength of the associated channel and  $t$  is the time. Further we assume but not underline a discrete character of  $\lambda$ .



and a dispersion of  $1 \text{ \AA}/\text{channel}$  is assumed) can be determined automatically and the desirable polynomial can be fitted. The normalized bins are

$$R_j(\lambda) = \frac{S_j(\lambda)}{C_j(\lambda)}, \quad (\text{A17})$$

where  $j = 1, 2, \dots, k$ .

The conversion of the spectra in every bin to relative units  $R_j(\lambda)$  suppresses all broad-band spectral variations. One can rewrite the formulae (A14,A15) for calculations of the Fourier coefficients in relative units

$$A(\lambda, P) = \frac{2}{k} \cdot \sum_{j=1}^k R_j(\lambda) \cos\left(\frac{2\pi}{k} \cdot j\right), \quad (\text{A18})$$

$$B(\lambda, P) = \frac{2}{k} \cdot \sum_{j=1}^k R_j(\lambda) \sin\left(\frac{2\pi}{k} \cdot j\right). \quad (\text{A19})$$

The power of spectral oscillations is

$$|X(\lambda, P)|^2 = A(\lambda, P)^2 + B(\lambda, P)^2. \quad (\text{A20})$$

In this consideration we have shown how to convert the result of data folding in the power of oscillations in relative units.

The basic idea of our algorithm is freedom in the choice of the spectrum parameter such as the integration time ( $\Delta t$ ). It means that it is possible for every period of interest  $P$  in the range

$$k \cdot dt \leq P \leq T, \quad (\text{A21})$$

where  $dt = 32 \text{ ms}$  and  $T$  is the time of exposure, to define  $\Delta t = \frac{P}{k}$  and to integrate spectra from the original data (a file with coordinates of photons) with an accuracy limited by  $dt = 32 \text{ ms}$ . Now we formulate this simple algorithm as:

1. The choice of the number of bins (it depends on an astrophysical problem), for example, this number is  $k = 10$ .
2. The choice of the periods of interest in the region (it also depends on an astrophysical problem), for example,  $P_1 = 600s, P_2 = 610s, \dots, P_i, \dots, P_{61} = 1200s$ .
3. For every period of interest BEGIN :

3.1 Spectrum integrations from the original data with

$$\Delta t = \frac{P_i}{k} \quad (\text{A22})$$

and data folding in  $k = 10$  bins. Every bin contains two spectra (object and sky).

3.2 Subtraction of a sky spectrum in every bin and conversion of every bin to relative units (normalization to continuous spectrum)

$$R_j(\lambda) = \frac{S_j(\lambda)}{C_j(\lambda)}, \quad (\text{A23})$$

where  $j=1,2,\dots,k$ .

3.4 Calculation of the power (or amplitude, phase) in relative units (A18,A19,A20) for every channel (wavelength) in the spectrum.

3.5 GO TO 3.1. For all periods ( $P_i$ ) of interest.

4. As a result we obtain a dependence of the power of oscillations on the wavelength and on the period in the desirable range  $|X(\lambda, P_i)|^2$ .

## References

- Afanasiev V.L., Lipovetskij V.A., Mikhailov V.P., Nazarov E.A., Shapovalova A.I., 1991, *Astrofiz.Issled.(Izv. SAO)*, 31, 128.
- Bonnet-Bidaud J.M., Mouchet M., Somova T.A., Somov N.N., 1996, *A&A*, 306,199
- Buckley D.,Tuohy I., 1989, *ApJ*, 344, 376.
- Buckley D.,Tuohy I., 1990, *ApJ*, 349, 296.
- Chanan G.A., Nelson J.E., Margon B., 1978, *ApJ*, 226, 963.
- Drabek S.V., Kopylov I.M., Somov N.N., Somova T.A., 1986, *Astrofiz.Issled.(Izv. SAO)*, 22, 64.
- Helditch R. W., Bell S.A. , 1994, *MNRAS*, 266, 703.
- Hellier C., Mason K.O., Rosen S.R, Cordova F.A., 1987, *MNRAS*, 228, 463.
- Hellier C., Mason K.O., Cropper M.S., 1990, *MNRAS*, 242, 250.
- Hellier C., Mason K.O., 1990, in *Accretion-Powered Compact Binaries*, ed. C.Mauché (Cambridge, Cambridge University), p.185.
- Hellier C., Cropper M.S., Mason K.O., 1991, *MNRAS*, 248, 233.
- Hellier C., Ramseyer T.F., Jablonski F.J., 1994, *MNRAS*, 271, L25.
- Henry R.J.W., O'Connell R.F., 1985, *PASP*, 97, 333.
- Ioannisian B.K. et al. , 1982, in: *Instrumentation for Astronomy with Large Optical Telescopes*, ed. C.M. Humphries, Reidel, p.3.
- Kemic S.B., 1974, in: *Joint Institute for Laboratory Astrophysics Report*, No 113, University of Colorado.
- Kopylov I.M., Somov N.N., Somova T.A., 1986, *Astrofiz.Issled.(Izv. SAO)*, 22, 77.
- Martell P.J., Horne K., Price G.M., Gomer R.H., 1995, *ApJ*, 448, 380.
- Mason K.O., Watson M.G., Ponman T.J., Charles P.A., Duck S.R., Hassall B.J.M., Howel S.B., Ishida M., Jones D.H.P., Mittaz J.P.D., 1992, *MNRAS*, 258, 749.
- Najdenov I.D., Panchuk V.E., 1996, *Bull. Spec. Astrophys. obs.*, 41, 145.
- Patterson J., 1994, *PASP*, 106, 209.
- Penning W.R., 1985, *ApJ*, 289, 300.
- Pirolla V., Hakala P., Coyne G.V., 1993, *ApJ*, 410, L107.
- Preston G.W., 1970, *ApJ*, 160, L143.
- Saffer R.A., Liebert J., Wagner R.M., Sion E.M., Starrfield S.G., 1989, *ApJ*, 98, N2, 668.
- Rosen S.R., Mittaz J.P.D., Hakala P.J., 1993, *MNRAS*, 264, 171.
- Somova T.A., Somov N.N., Markelov S.V., Nebelitskiy V.B., Spiridonova O.I., Fomenko A.F., 1982, in: *Instrumentation for Astronomy with Large Optical Telescopes*, ed. C.M. Humphries, Reidel, 283.
- Somov N.N., 1986, *Astrofiz. Issled. (Izv. SAO)*, 22, 73.
- van der Klis M., 1989. In: *Timing Neutron Stars*, NATO ASI Ser. C, H. Ogelman, E.P.J. van den Heuvel (eds), Dordrecht:Kluwer, vol. 262, p. 27